JOURNAL OF SPACECRAFT AND ROCKETS
Vol. 35, No. 2, March–April 1998

Navier–Stokes Analysis of Subsonic Flowfields over a Missile Configuration

Ismail H. Tuncer* and Max F. Platzer†
U.S. Naval Postgraduate School, Monterey, California 93943
and
Robert D. VanDyken‡
U.S. Naval Air Warfare Center, China Lake, California 93555

Subsonic flowfields over a missile configuration are computed at high angles of attack ranging from 15 to 60 deg with the NASA Ames Research Center OVERFLOW Navier–Stokes solver. The computed flowfields are presented in terms of particle traces, helicity contours, and surface streamlines. The flow separation over the missile body, the development of leeward-side vortex patterns, and the canard and tail vortices and their interaction are identified. The computed normal force and pitching moment coefficients compare well with the experimental data at an incidence of 15 deg. At higher incidences the normal force is underpredicted by up to 15%. The computed pitching moments agree qualitatively well with the experimental data, but percentage deviations are substantial in the higher incidence range.

Nomenclature

C_M = pitching moment coefficient
C_N = normal force coefficient
D = diameter of missile body
M_∞ = freestream Mach number
Re_D = Reynolds number based on diameter D
α = incidence angle
γ = canard deflection angle

Introduction

THE flow over a full missile configuration with canards and tails at high angles of attack is highly complex because of flow separation and formation of canard and body vortices and their interaction. Studying the complex flowfield and understanding the effect of the canards on the performance, stability characteristics, and development of flow asymmetries are crucial to efforts to design future missile airframes. This work is aimed at utilizing the current computational fluid dynamics methods for investigating the complex flowfields and validating the computed results with experimental data.

Investigations on the aerodynamic characteristics of canard-controlled missiles at high angles of attack are of considerable interest because future combat aircraft may have the capability to maintain controlled flight at low speeds and high incidence angles. Therefore, in this flight regime missiles may be launched at a large angle of attack in contrast to traditional launches at angles of attack of no more than 10–15 deg. The resulting high-angle-of-attack flowfield over a missile is vortex dominated with vortex breakdown and asymmetric vortex flow behavior, which lead to unpredictable aerodynamic forces and pose a potential threat to flight stability. Thus, a better understanding of the missile aerodynamics at high angles of attack is needed to expand missile launch windows and to improve future missile designs.

The current design tools for missile airframes range from semiempirical methods to Navier–Stokes solvers.[1,2] A recent comprehensive review of high-angle-of-attack aerodynamics has been given by Rom.[1] Recent Navier–Stokes computations[3–7] of flowfields around complete aircraft and missile configurations at high angles of attack show encouraging agreement with available experimental data. Schiff and colleagues[3,4] studied flows over a slender ogive-cylinder body of revolution at high angles of attack by solving the thin-layer Navier–Stokes equations. They calculated the growth of crossflow separation and the development of leeward-side vortex patterns, and they identified the unsteadiness of the flowfields at high angles of attack.

Recently, Ekaterinaris[5] and Hsieh et al.[6] studied a full missile configuration at low subsonic speeds and high angles of attack. Hsieh et al. used the GASP Navier–Stokes solver to compute laminar flows over the missile at 0-deg angle (+ configuration), 0-deg canard deflection, and 15-, 30-, 45-, and 60-deg angles of attack. Ekaterinaris[5] computed the turbulent flow over the same missile configuration at a 45-deg roll angle (X configuration) and a 45-deg angle of attack. These computations were found to be in good agreement with the experimental force and moment data obtained in the U.S. Naval Postgraduate School wind tunnel[8] and in the NASA Ames Research Center 7 × 10 ft wind tunnel.[9]

In this work, we build on the work of Ekaterinaris.[5] Subsonic flowfields around the missile configuration (Fig. 1) are computed by using the OVERFLOW Navier–Stokes solver. The computed flowfields between 15 and 60 deg are analyzed in terms of particle traces and surface streamlines. The integrated aerodynamic loads are compared with the experimental data.[9]

Numerical Method

Figure 1 shows the missile configuration studied. The missile is 22.6 diameters long. It has 67-deg swept delta canards with a root chord length of 2.5 diameters and 45-deg swept trapezoidal tails with a root chord length of 3 diameters. The tails are attached to the missile body and positioned parallel to the missile axis, whereas the canards are separated from the body by a small gap and can be set at a prescribed canard deflection, δ. The gap between the canard and the body, which becomes more distinguished when the canards are set at an angle, is taken into consideration during discretization of the computational domain.

The same missile configuration was also used in an experimental study conducted by Smith and Smith.[9] A one-third-scale model was sting-mounted on a precision balance. The presence of the sting was also taken into consideration in these computations.

The OVERFLOW Navier–Stokes solver (version 1.6ao) developed at NASA Ames Research Center[10,11] was used to solve viscous flowfields over the missile configuration. The computational domain, which consists of the missile body, the sting, and the canards

Presented as Paper 97-0635 at the AIAA 35th Aerospace Sciences Meeting, Reno, NV, Jan. 6–9, 1997; received March 24, 1997; revision received Aug. 16, 1997; accepted for publication Oct. 10, 1997.

*Research Assistant Professor, Department of Aeronautics and Astronautics. Member AIAA.
†Professor, Department of Aeronautics and Astronautics. Associate Fellow AIAA.
‡Research Scientist, Weapons Division. Member AIAA.

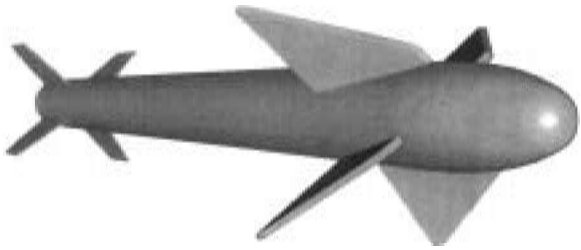

Fig. 1 Missile configuration at 10-deg canard deflection.

and the tails and the flowfield around them, is partitioned into zonal blocks. The zonal blocks are discretized with structured subgrids, which are overset onto each other. The OVERFLOW solver computes flowfields in each subgrid implicitly and interpolates the flow variables at the grid boundaries from the neighboring grids by using the interpolation data supplied by the PEGSUS code. The PEGSUS code is used as a preprocessor for the overset grids.

OVERFLOW Navier–Stokes Solver

OVERFLOW is a Reynolds-averaged, compressible Navier–Stokes solver. It accommodates computational domains discretized with overset grids, which are preprocessed with the PEGSUS code. The OVERFLOW code has several discretization and time integration schemes for each subgrid. In this study, for subgrids in which one of the (i, j, k) grid directions aligns with the freestream flow direction, the partial flux vector splitting algorithm is selected. Otherwise, the 3-factor diagonal scheme with central differencing is used. The partial flux vector splitting algorithm uses Steger–Warming flux vector splitting for discretization of the convection terms in the streamwise direction and central differencing in the other two directions. For the flux splitting algorithm, the central difference smoothing coefficient was gradually reduced to about 0.06 from the starting value of 0.10. For the central difference algorithm on the wing and canard grids, the fourth-order smoothing coefficient was similarly reduced to 0.08 from 0.1. The flowfield was assumed to be fully turbulent and the Baldwin–Lomax algebraic eddy viscosity model with Degani–Schiff cutoff was used. In cylindrical grids around the missile body, the thin-layer flow assumption was made, and only the viscous terms in the crossflow direction were considered. Local time stepping was used for convergence to a steady-state solution. The convergence criterion was based on the L2 norm of the residuals and the time variation of the integrated aerodynamic loads.

No-slip boundary conditions are applied at the solid surface boundaries. At the farfield boundaries, one-dimensional Riemann invariant extrapolation is used. At the intergrid boundaries, the flow variables are interpolated from the neighboring grids. The intergrid interpolation stencils and weights are input to the solver. The PEGSUS code is used as a preprocessor to determine the hole boundaries created by the overset grids in the outer grids and to obtain the intergrid interpolation stencils and the corresponding interpolation weights.

In the OVERFLOW code, the aerodynamic loads are based on the integration of surface pressure and skin friction coefficients. In these computations, the total aerodynamic loads are obtained by summing the integrated loads for subgrids with solid-surface boundary conditions. Note that this approach does not account for the overlapping grid regions on solid boundaries, which cover approximately less than 1% of the total solid surface area.

Computational Domain

In this study we considered only the flows at 45-deg roll angle (X configuration) and zero sideslip angle. The flowfield is therefore assumed to be symmetric with respect to the midplane, and only the computational domain over the half-missile configuration is discretized. The computational domain around the canards and the tails, the gaps between the canard and the body, and the zones over the missile body are discretized with structured subgrids. As shown in Fig. 2, 13 subgrids with a total of approximately 1×10^6 grid points are used.[5] The canard, the tail and gap grids, and the outer grids around them are relatively high-resolution viscous grids with clustered grid distributions around the leading edges. The y^+ values

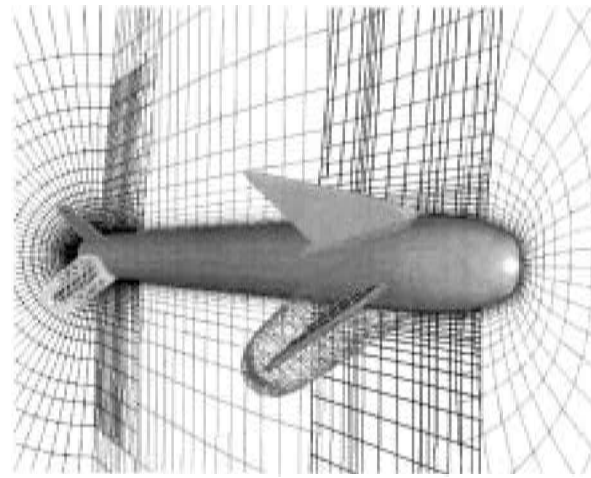

Fig. 2 Overset computational grid. (Every other grid point is plotted.)

were on the order of $\mathcal{O}(1)$ for all of the surface grids. The outer boundaries of the computational domain are located about five missile lengths away.

Results and Discussion

We have computed high-angle-of-attack, subsonic flowfields over the missile configuration at $\alpha = 15$-, 25-, 30-, 45-, and 60-deg incidences; $M_\infty = 0.3$; and $Re_D = 0.95 \times 10^6$, where the Reynolds number is based on the diameter of the missile body. Flowfields were assumed to be steady, and the local time-stepping option in the OVERFLOW solver was used to converge to a steady-state solution. All of the computations were carried out on remote Cray Y-MP and Cray C90 supercomputers. A typical computation took about 6000–8000 time steps and 30–40 CPU h on a Cray Y-MP.

The FAST flow visualization software from NASA Ames Research Center was used for postprocessing the flowfield data. The computed flowfields were analyzed in terms of particle traces, helicity contours, and surface streamlines. Helicity is defined as the dot product of velocity and vorticity vectors, which emphasizes the vorticity in the flow direction.

In addition, the integrated aerodynamic loads were compared with the experimental data[9] and the semiempirical predictions by the missile DATCOM. A series of experiments was performed in the NASA Ames Research Center 7×10 ft subsonic wind tunnel with a one-third-scale model of the same missile configuration.[9] The model was fitted with boundary-layer transition strips at the nose and the canard and tail fin leading edges. The normal, side, and axial forces and the pitching, rolling, and yawing moments were measured by means of a six-component, strain gauge-type balance. The tests were performed at $M_\infty = 0.15$.

The missile DATCOM is a semiempirical program originally developed by McDonnell Douglas to calculate the static stability and control characteristics of various missile configurations. It uses analytic methods with experimental data substitution to predict integrated aerodynamic loads.

Figure 3 shows the flowfield computed at $\alpha = 15$ deg. As observed in the particle traces and the helicity contours, the flow stays mostly attached over the forebody and the main missile body except over the canard and tail sections. The leeward-side flow over the canards and the tails separates at the leading edges, forming leading edge vortices. The leading edge vortices are also depicted by the flow reattachment and the secondary flow separation lines parallel to the leading edges in the surface streamlines. The trajectories and the interaction of the canard vortices are captured in the helicity contours. It is observed that, as a result of the interaction, the canard vortices roll up in the clockwise direction. It also appears that the upper canard vortex induces a strong downwash on the leeward side of the missile and suppresses the leeward-side flow separation behind the canards.

Because the gap between the canards and the missile body is modeled, the flow is allowed to pass through the gap as observed in the surface streamlines. However, a vortical corner flow still develops

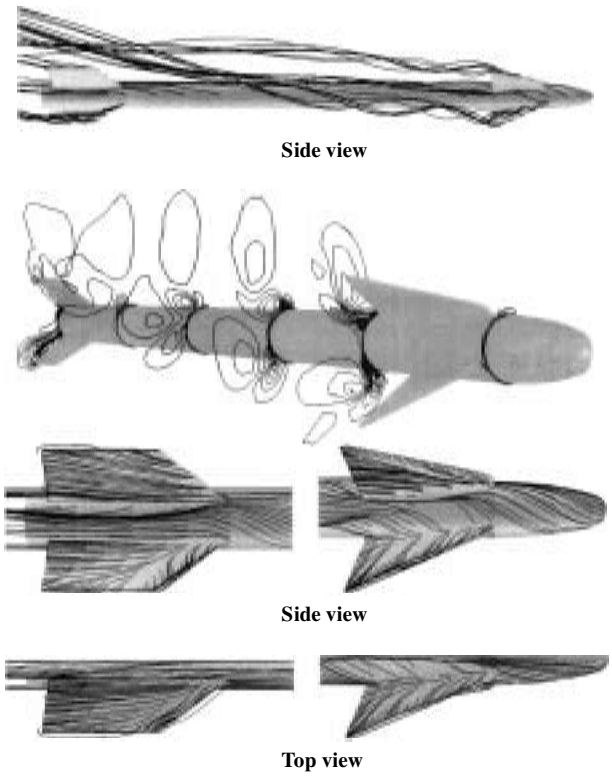

Fig. 3 Particle traces, helicity contours, and surface streamlines at forebody and tail sections at α = 15 deg.

below the canard-body junction as observed in the helicity contours. These vortices stay close to the missile body and roll up with the canard vortices as they are convected downstream.

The tail vortices originating from the leading edges of the tails appear to be smaller and weaker than the canard vortices. The separated flow zone at the leeward side of the upper tail is also smaller than that of the lower tail, and the flow stays mostly attached. This is attributed to the smaller angle of attack the upper tail sees.

At $\alpha = 30$ deg, the flowfield (Fig. 4) in general is similar to that of $\alpha = 15$ deg except the leeward-side flow separates at the forebody as well. Also, in the helicity contours, which are plotted in the same range, the leeward-side vortices over the missile body are stronger and the recirculating regions grow larger. Comparison of surface streamlines with the experimental paint flow visualization at $\alpha = 25$ deg is shown in Fig. 5. The experimental surface paint data are not very clear over the forebody. Nevertheless, the secondary flow separation lines over the canards and the tails, the flow separation over the missile body, and the flow reattachment over the tails are in good qualitative agreement, except experiments indicate that the secondary separation line on the lower tail is located farther away from the side edge.

The flowfield computed at $\alpha = 45$ deg (Fig. 6) exhibits a qualitative change. In contrast to previous cases, the coherent leading edge vortices over the lower canard and tail are no longer observed. On the lower canard, the flow that separates at the leading edge hits the lower surface of the upper canard before it can ever reattach on the upper surface. On the lower tail, the reattachment of the flow is not observed either. Instead a corner vortex originating from the apex develops. The separated flow at the leading edge reattaches on the lower surface of the upper tail as shown in the surface streamlines. On the other hand, the leading edge vortices still develop over the upper canard and the tail, and the primary flow reattachments are observed close to the root. The leeward-side vortex over the forebody and the missile body and over the upper tail grows stronger. The flow separation on the leeward side of the forebody also moves closer to the symmetry plane under the influence of the gap flow.

Figure 7 shows the flowfield computed at $\alpha = 60$ deg. Besides the larger recirculation regions on the leeward side of the missile body, the flowfield shows characteristics similar to that at $\alpha = 45$ deg.

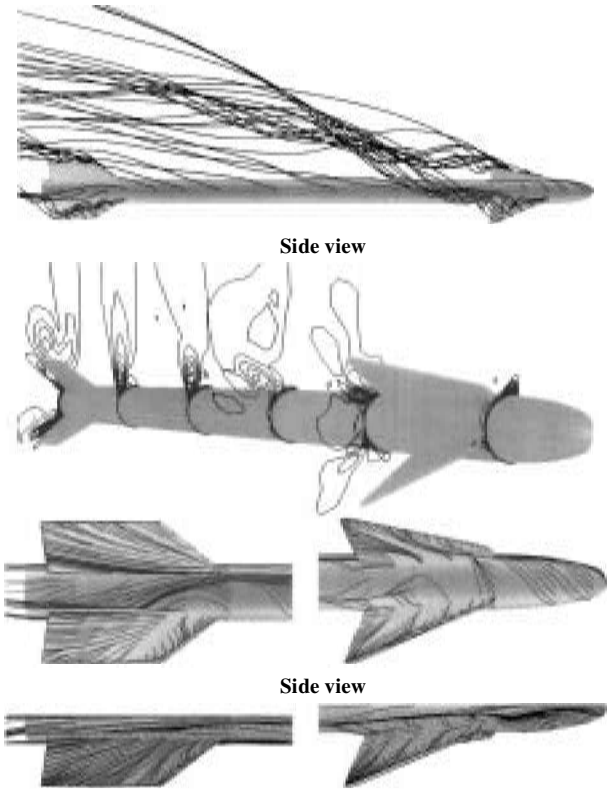

Fig. 4 Particle traces, helicity contours, and surface streamlines at forebody and tail sections at α = 30 deg.

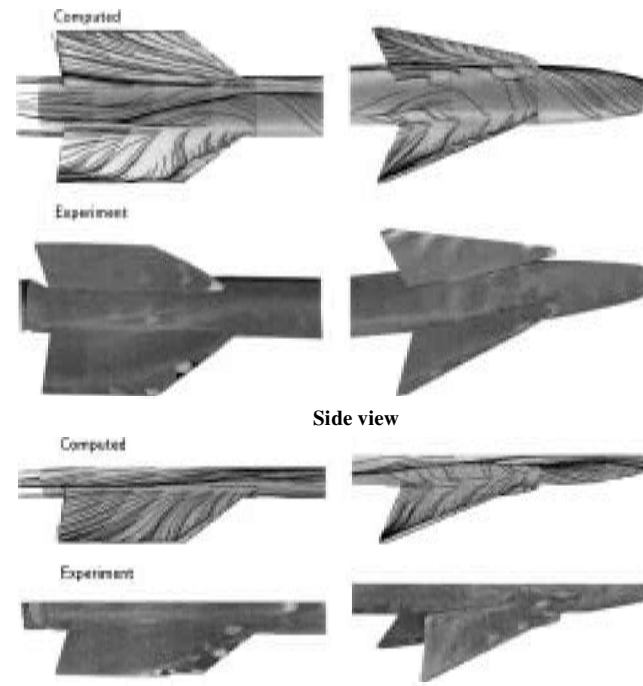

Fig. 5 Computed and experimental surface streamlines at forebody and tail sections at α = 25 deg.

The computed normal force and pitching moment coefficients are presented in Fig. 8. The pitching moment convention is positive nose-up and is with respect to the center of gravity, which is located 11.5 diameters from the missile nose. The reference area is the cross-sectional area of the missile body. Although the normal force is underpredicted and the moment stall is delayed at angles of attack greater than 30 deg, the computed values agree well qualitatively with the experimental data and the DATCOM predictions.

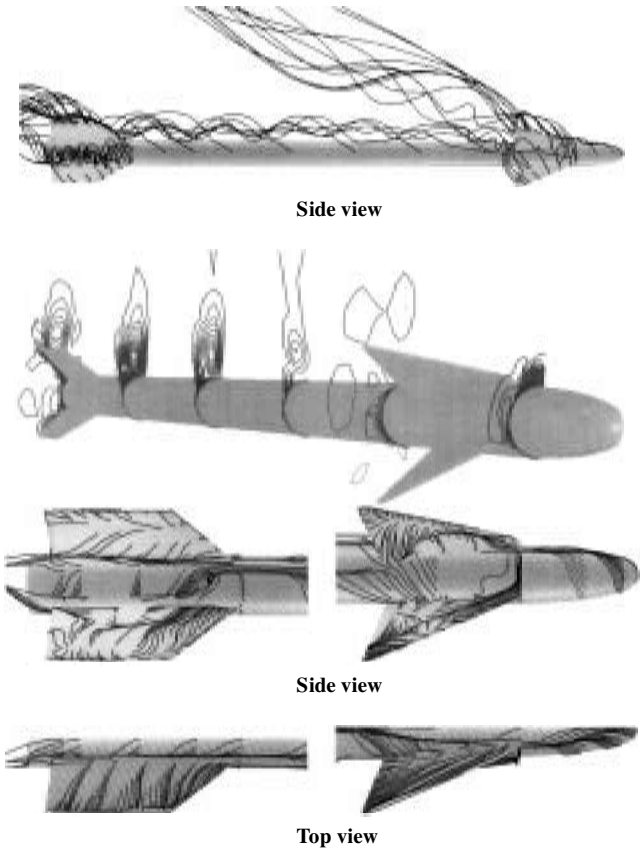

Fig. 6 Particle traces, helicity contours, and surface streamlines at forebody and tail sections at $\alpha = 45$ deg.

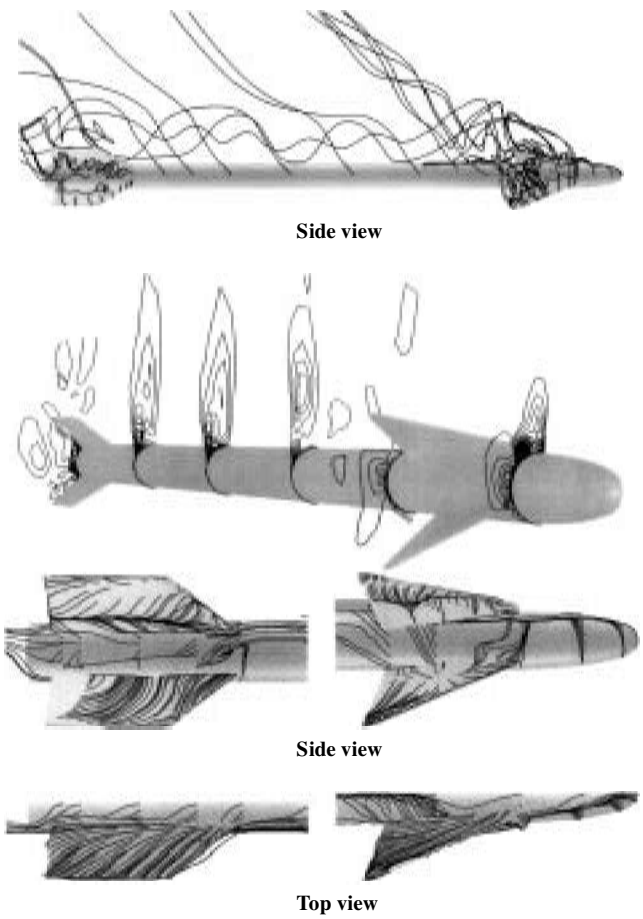

Fig. 7 Particle traces, helicity contours, and surface streamlines at forebody and tail sections at $\alpha = 60$ deg.

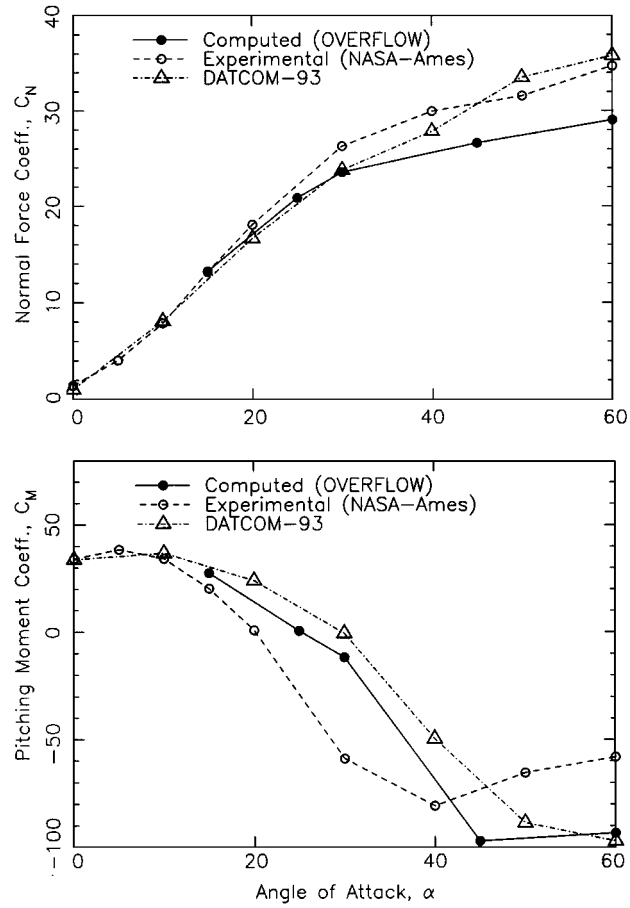

Fig. 8 Aerodynamic loads at $\delta = 10$ deg, $M = 0.3$, and $Re_D = 0.95 \times 10^6$.

The delay in the predicted pitching moment stall suggests that the loss of suction on the canard surfaces and the missile forebody is underpredicted in the computations. The leveling off of the moment coefficient at angles of attack greater than 40 deg, which is captured in the computations, is attributed to the massive flow separation and the stall over the canards, tails, and missile forebody.

The same flowfield at 45 deg was also computed by Ekaterinaris.[5] Although the computed flowfields show similar characteristics, the computed normal force and pitching moment coefficients are given in Ref. 5 as 32.7 and −71.9, respectively, in contrast to 26.6 and −97.1 in these computations. Further work is necessary to identify the precise reasons for this discrepancy.

Conclusions

A Navier–Stokes solver with overset grids, OVERFLOW, was used to compute the subsonic flowfields over a missile configuration at high angles of attack ranging from 15 to 60 deg. The canard and tail vortices, their interaction, and the flow separation over the missile body are identified. The computed normal force and pitching moment coefficients agree well with the measurements at a 15-deg angle of attack, but the normal force predictions deviate by up to 15% at the higher incidences. The pitching moment predictions show larger percentage deviations from the experiment at the higher angles of attack. However, the qualitative trends are correctly predicted, showing improvement over the DATCOM predictions. Further computations are needed to explore the unsteadiness of the flow and the asymmetric vortex shedding at high incidences, the effect of higher-order turbulence models, the inclusion of boundary-layer transition models, and the grid sensitivity. Also, detailed flowfield measurements are needed for the ultimate assessment of computational accuracy instead of comparisons with total force and moment measurements.

Although the computations are CPU intensive and convergence for separated flows is slow, the OVERFLOW Navier–Stokes solver

with overset grids is an effective tool for analysis of separated vortical flowfields over full missile configurations.

Acknowledgments

This work was supported in part by a grant of high performance computing (HPC) time from the U.S. Department of Defense HPC Centers at Vicksburg (Cray Y-MP) and Stennis (Cray C90). The authors are grateful to J. A. Ekaterinaris for providing the computational grid. We also thank David Siegel, Office of Naval Research, and Craig Porter and C. Housh, Weapons Division, U.S. Naval Air Warfare Center, China Lake, for their support of this project.

References

[1]Rom, J., *High Angle of Attack Aerodynamics*, Springer–Verlag, New York, 1992.

[2]Hemsch, M. J., and Nielsen, J. N. (eds.), *Tactical Missile Aerodynamics*, Vol. 104, Progress in Astronautics and Aeronautics, AIAA, New York, 1986, Chaps. 7, 11–13, and 15.

[3]Degani, D., and Schiff, L. B., "Computation of Turbulent Supersonic Flows Around Pointed Bodies Having Crossflow Separation," *Journal of Computational Physics*, Vol. 66, No. 1, 1986, pp. 173–196.

[4]Schiff, L. B., Degani, D., and Gavali, S., "Numerical Simulation of Vortex Unsteadiness on Slender Bodies of Revolution at Large Incidence," AIAA Paper 89-0195, Jan. 1989.

[5]Ekaterinaris, J. A., "Analysis of Flowfields over Missile Configurations at Subsonic Speeds," *Journal of Spacecraft and Rockets*, Vol. 32, No. 3, 1995, pp. 385–391.

[6]Hsieh, T., Priolo, F. J., and Wardlaw, A. B., Jr., "Navier–Stokes Calculation of Flow over a Complete Missile to 60 Degree Incidence," AIAA Paper 95-0760, Jan. 1995.

[7]Tuncer, I. H., Marvin, R., and Platzer, M. F., "Numerical Investigation of Subsonic Flow over a Typical Missile Forebody," AIAA Paper 96-0189, Jan. 1996.

[8]Smith, E. H., Hebbar, S. K., and Platzer, M. F., "Aerodynamic Characteristics of a Canard-Controlled Missile at High Angles of Attack," *Journal of Spacecraft and Rockets*, Vol. 31, No. 5, 1994, pp. 766–772.

[9]Smith, B. E., and Smith, E. H., "High Angle-of-Attack Wind Tunnel Test in NASA Ames 7 by 10 Foot Wind Tunnel," U.S. Naval Air Warfare Center–Weapons Div., NAWC–WD Rept., China Lake, CA, Sept. 1992.

[10]Ying, S. X., Steger, J. L., Schiff, L. B., and Baganoff, D., "Numerical Simulation of Unsteady, Viscous High-Angle-of-Attack Flows Using a Partially Flux-Split Algorithm," AIAA Paper 86-2179, June 1986.

[11]Benek, J. A., Buning, P. G., and Steger, J. L., "A 3D Chimera Grid Embedding Technique," AIAA Paper 85-1523, July 1985.

R. M. Cummings
Associate Editor